Matter

CellPress

Article

Bio-inspired construction of ion conductive pathway in covalent organic framework membranes for efficient lithium extraction

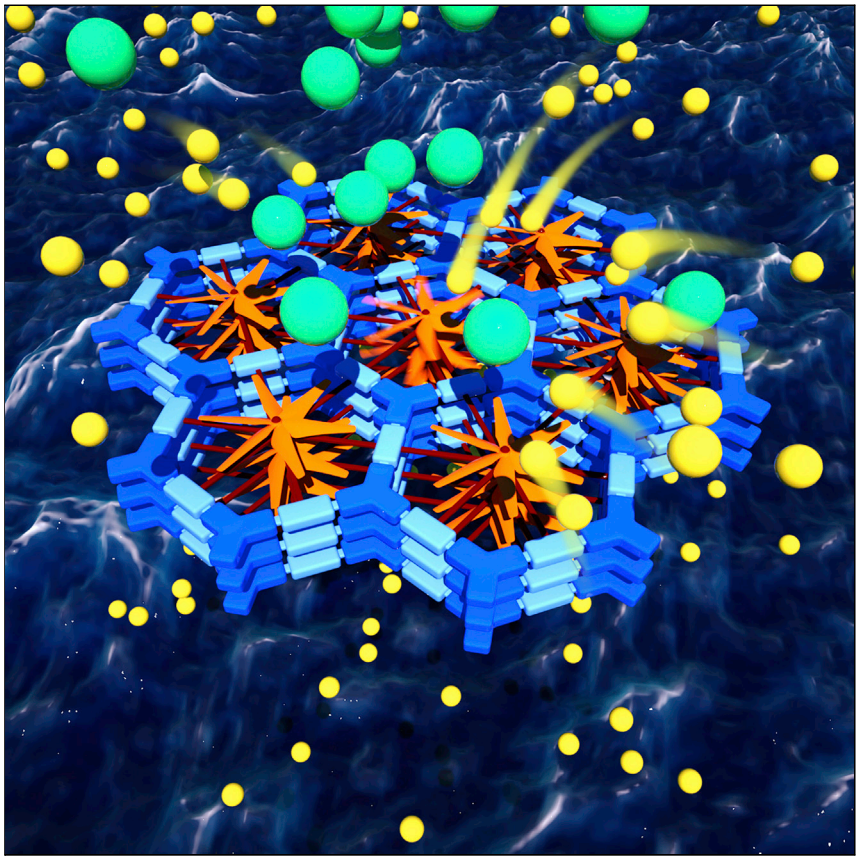

By virtue of their tailorable pore environment and unique pore structure, 2D COFs serve as excellent candidates for exploring biomimetic ion channels for sophisticated separation. The 1D pore structure offers unidirectional pathways for swift ion diffusion, wherein the aligned lithiophilic oligoethers oriented in close proximity further facilitate Li ion transport but obstruct the other ions from entering the channel, resulting in a high Li^+/Mg^{2+} separation factor of up to 64.

Shaosuo Bing, Weipeng Xian, Sifan Chen, ..., Shengqian Ma, Qi Sun, Lin Zhang

sunqichs@zju.edu.cn (S.M.)
shengqian.ma@unt.edu (Q.S.)

Highlights

An alternative Li^+/Mg^{2+} separation mechanism by membrane is proposed

Oligoethers facilitate Li^+ transport but obstruct other ions from entering

The oligoethers on the COF act as relay parts to transport Li^+ by charge repulsion

Pore-environment engineering represents a new addition to enhance membrane properties

Improvement
Enhanced performance with innovative design or material control

Bing et al., Matter 4, 2027–2038
June 2, 2021
https://doi.org/10.1016/j.matt.2021.03.017

Matter

CellPress

Article

Bio-inspired construction of ion conductive pathway in covalent organic framework membranes for efficient lithium extraction

Shaosuo Bing,[1] Weipeng Xian,[1] Sifan Chen,[1] Yanpei Song,[2] Linxiao Hou,[1] Xiaolong Liu,[3] Shengqian Ma,[2,*] Qi Sun,[1,4,*] and Lin Zhang[1]

SUMMARY

As the most sophisticated separation system, biological membranes have served as natural prototypes for the design of artificial membranes because they provide high permeability and solute selectivity, owing to the presence of specialized ion channels. However, developing stable and selective artificial ion channels remains a formidable challenge. Herein, we demonstrate the construction of lithium nanochannels in two-dimensional covalent organic frameworks (COFs) to create biomimetic membranes. Implanted lithiophilic oligoethers conferred specificity and facilitated Li^+ diffusion along the pore pathway of the COF. The ion channel characteristics were indicated by reversal potential measurements, showing that the relative permeability decreased in the order $Li^+ > K^+ > Na^+ > Ca^{2+} > Mg^{2+}$. The Li^+ transfer was enhanced, while other ions were obstructed, allowing for high selectivity and permeability. A Li^+/Mg^{2+} separation factor of 64 was achieved, confirming high lithium affinity. This study may serve as a design principle to develop selective artificial membranes for effective ion separation.

INTRODUCTION

The desire to mimic cell membranes with meticulous control over ion transport has attracted significant research interest for decades.[1–3] The spatially well-arranged binding sites in ion channels enable rapid transport and high selectivity. However, most synthetic membranes that are capable of discriminating ions are functionalized with charged moieties.[4–11] The main underlying principle for ion selectivity across these membranes is Donnan exclusion, whereby the membranes reject co-ions as the excess charge and transport counter-ions.[12,13] Because of the charge repulsion involved in the separation process, the transport of co-ions slows down when approaching a charged membrane. Therefore, there is a need to develop novel separation layers to achieve active separation. We investigated the possibility of accelerating the transport of target ions across the membrane while lowering the diffusion of other ions to achieve a high selectivity similar to that seen in nature.

Lithium has become an essential resource for modern society because of the growing demand for lithium batteries in portable electronic devices and vehicles. This has rendered lithium availability a matter of energy security and the development of efficient lithium extraction technologies a growing area of interest.[14,15] Given that lithium is widely distributed in salt-lake brines, considerable efforts have been made in lithium extraction (Table S1).[16–18] State-of-the-art positively charged nanofiltration membranes show a satisfactory Li^+/Mg^{2+} separation factor of up to 10, a critical requirement for

Progress and potential

With lithium batteries expected to increase over the coming decades, access to this reserve is imperative for future energy storage devices. Substantial effort has been expended to develop membrane-based technologies to extract lithium from salt-lake brines, but the very similar reactivities of Li^+ and Mg^{2+} make this a challenging task. Herein, we show how two-dimensional covalent organic frameworks (COFs) possess all the necessary traits to create ideal membranes for Li extraction. The COF active layer with orderly aligned oligoethers in the pore channels affords a high Li^+/Mg^{2+} separation factor of 64, going into a top rank in terms of extraction efficiency. The lithiophilic oligoethers show a pumping feature that accelerates the Li^+ transfer in the pore channels, defeating the trade-off between selectivity and permeability. These findings represent a promising addition to the rapidly increasing arsenal of energy material harvesting.

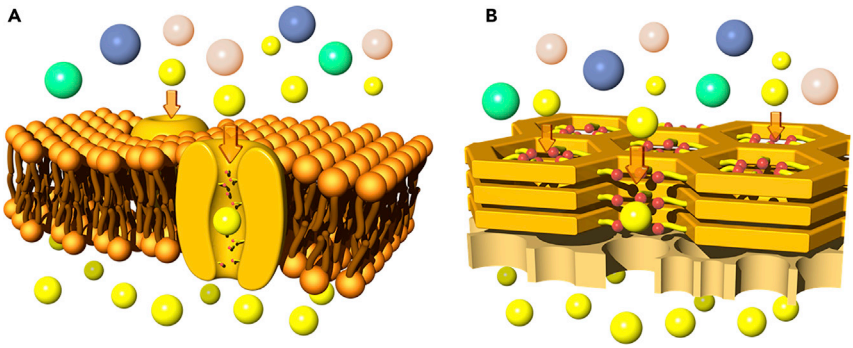

Figure 1. Conceptual scheme

(A) Diagrammatic sketch of ion channels in nature.

(B) Schematic illustration of the construction of lithium channels using a 2D COF as a designer platform by implanting lithiophilic functionalities. The Li ion transfer was enhanced, while other ions were obstructed, allowing for high selectivity as well as permeability.

achieving high-grade Li_2CO_3.[19–21] To develop new synthetic Li^+ transporters, we postulated introducing lithiophilic functionality into membranes to lower the energy barrier for lithium passage and hence the accompanied selectivity. Prior studies revealed that polyethylene oxide moieties could coordinate and transport Li^+ for the design of a new type of solid-state polyelectrolyte,[22–27] and we looked into implementing the same functionality into porous membranes. This approach was aimed at combining the benefits of the innate porosity of the membranes with the affinity of the ether moieties toward Li^+ to form a lithium highway, ultimately resulting in a high lithium extraction efficiency. We envisioned two-dimensional (2D) covalent organic frameworks (COFs) as promising candidates for active layers to achieve these goals.[28–48] In contrast to the current nanofiltration membranes, which are optimized empirically, COFs, with the advantage of high modularity, can potentially form active layers with designable pore structures and tunable functionality. Further, the discogens of 2D COFs are arranged in a columnar fashion, owing to the strong π-π interactions between aromatic cores and the aligned lithiophilic functionalities oriented in close proximity, offering unidirectional pathways for swift ion diffusion and enhanced communication between adjacent ions in the queue (Figure 1).

In this contribution, we show that COF-based membranes implanted with oligoethers can indeed provide an ion-diffusion pathway. The transport of Li ions is accelerated by rapid and reversible coordination with the ether moieties, thereby differentiating Li ions from other ions. Theoretical and spectroscopic studies were carried out to explain the observed selective extraction efficiency based on the interaction and dynamic exchange between oligoethers and Li ions. The synergistic effect between the densely populated lithiophilic sites and the 1D channels promotes significantly faster ion transport rates and allows the use of thicker films. The performance is very stable, as reflected by the fact that the selectivity is retained under the same conditions for at least 40 h. Our studies indicate that pore-environment engineering by introducing lithiophilic functionalities could be a promising strategy to optimize the separation performance of membranes that circumvent the issues of current ones that require trade-offs in properties.

RESULTS

Membrane fabrication and characterization

We selected 1,3,5-tris(4-aminophenyl)benzene (TAB) as the base for the construction of COF membranes because the resulting COFs have not only been proven to be stable under a wide range of conditions, but also possess high crystallinity

[1]Zhejiang Provincial Key Laboratory of Advanced Chemical Engineering Manufacture Technology, College of Chemical and Biological Engineering, Zhejiang University, Hangzhou 310027, China

[2]Department of Chemistry, University of North Texas,1508 W Mulberry Street, Denton, TX, 76201, USA

[3]School of Materials, Sun Yat-Sun University, Guangzhou 510006, China

[4]Lead contact

*Correspondence: sunqichs@zju.edu.cn (S.M.), shengqian.ma@unt.edu (Q.S.)

https://doi.org/10.1016/j.matt.2021.03.017

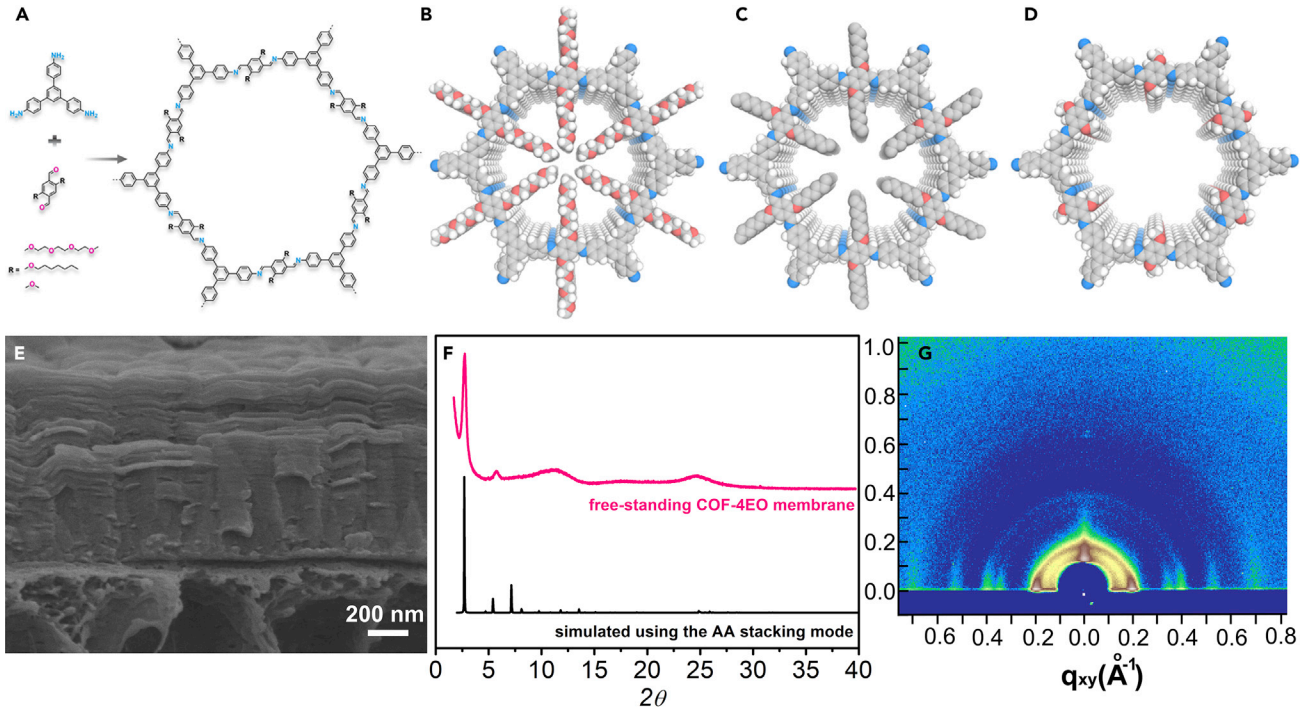

Figure 2. Structure and morphology characterizations

(A) Synthetic scheme of COFs with various pour environments through the condensation of TAB with various dialdehyde compounds.

(B, C, and D) Graphic views of the slipped AA stacking structure of (B) COF-4EO, (C) COF-OHep, and (D) COF-OMe, respectively (blue, N; gray, C; pink, O; white, H).

(E) Cross-sectional SEM image for COF-4EO-PAN.

(F) PXRD patterns (the free-standing COF-4EO membrane was achieved by dissolving the PAN support).

(g) GIWAXS pattern for COF-4EO-PAN.

as well as geometrical compatibility with various aldehyde counterparts, enabling us to optimize the composition within a single COF family (Figures 2A–2D).[49,50] To construct lithium channels, we paired TAB with an aldehyde monomer bearing oligo(ethylene oxide) chains, 2,5-bis(2-(2-(2-methoxyethoxy)ethoxy)ethoxy)terephthalaldehyde (4EO) (Figure 2B), as previous X-ray diffraction study revealed that in a polyethylene oxide-Li complex, there are four ether oxygens coordinated to each Li ion.[51] To reveal the role of oligoether moieties and exclude the impact of channel congestion resulting from the introduced substituted group, TAB was also paired with 2,5-bis(heptyloxy)terephthalaldehyde (OHep) for comparison (Figure 2C). To confer stability and processibility to the COF-based membranes, we grew COF active layers on polyacrylonitrile (PAN) ultrafiltration membranes via interfacial polymerization (Figure S1).[52] The choice of PAN as the substrate was made because it is flexible, which can increase the operability, and it is hydrophilic and negatively charged, which can lower the transmembrane energy of cations. To facilitate the reaction at the interface of PAN, an aqueous solution of acetic acid and amine monomers and an organic phase with aldehyde monomers were separately introduced into two sides of a diffusion cell, with the resulting membranes denoted as COF-4EO-PAN and COF-OHep-PAN (Figure S2). The characterization results of COF-4EO-PAN are discussed here, while the corresponding results for COF-OHep-PAN are detailed in the supplemental information (Figures S3–S7).

The morphologies of the as-prepared COF-4EO-PAN were examined by scanning electron microscopy (SEM). Compared with the pristine PAN, the SEM images of

COF-4EO-PAN showed several notable features (Figure S8). Cross-sectional SEM images of pristine PAN and COF membranes revealed distinct regions with different morphologies. COF-4EO-PAN was composed of multiple nanosheets, which were stacked layer by layer into a highly regular and lamellar structure with a thickness of approximately 1 μm (Figures 2E, S9, and S10). The top view of the SEM image of COF-4EO-PAN revealed that the PAN support was completely covered with a layer of COF material. The Fourier transform infrared (FTIR) spectra of both the TAB and the dialdehyde monomers, and the free-standing COF membrane, which was achieved by dissolving the PAN support in dimethylformamide, are shown in Figure S10. In contrast to the spectra of TAB and 4EO, no peaks were observed in the primary amine region (3,440 and 3,350 cm^{-1}) or at 1,685 cm^{-1}, corresponding to the carbonyl group, in the spectrum of the COF membrane. Together with the appearance of the characteristic C=N band at 1,614 cm^{-1}, this suggests the formation of a COF layer and that no detectable monomers are trapped in the membrane (Figure S11).[53] Moreover, the peak ascribed to the aldehyde group at around 170 ppm disappeared in the solid-state ^{13}C nuclear magnetic resonance (NMR) spectrum of the free-standing COF-4EO membrane, further supporting the aforementioned claim (Figure S12). The powder X-ray diffraction (PXRD) pattern of the free-standing COF membrane showed several prominent diffraction peaks suggestive of its high crystallinity (Figure 2F). To determine the structure, we used Materials Studio, which revealed that the experimental powder patterns were well matched with the optimized *p6m* symmetric structure model in eclipsed AA stacking (Tables S2–S4). The porosity of the membrane was evaluated by N_2 sorption isotherms, showing that COF-4EO possessed a Brunauer-Emmett-Teller surface area of 837 $m^2\ g^{-1}$ and a pore size of 2.34 nm (Figure S13). To gain insight into the extent of the alignment of the COF layer on PAN, we performed grazing-incidence wide-angle X-ray scattering (GIWAXS) measurements, which indicated that COF-4EO-PAN had a (001) direction perpendicular to the substrate (Figure 2G).[54] Therefore, we successfully prepared a COF active layer with its 2D plane flat on the substrate, where the oligo(ethylene oxide) chains vertically line the pore walls.

Ion transport characterization

To demonstrate the ion channel characteristics of the resulting membranes, we investigated the relative permeativity of various ions by measuring the reversal potentials. Tests were carried out on a bi-ionic system separated by the COF membranes. A $MgCl_2$ solution was introduced on the *cis* side, and various metal chlorides, such as NaCl, KCl, LiCl, $MgCl_2$, or $CaCl_2$, were placed on the *trans* side (facing the COF layer). To evaluate the relative permeativity of cations exclusively, the concentrations of Cl ions were kept the same. From the x intercepts of the current traces plotted against voltages, the reversal potentials were obtained.[55] When the *trans* side was filled with $MgCl_2$, the resulting current-voltage curves passed almost through the origin, suggesting that both COF-4EO-PAN and COF-OHep-PAN showed nearly equal permeabilities on both sides. Reversal potentials of 21.2, 17.7, 8.8, and 2.5 mV were observed for LiCl, KCl, NaCl, and $CaCl_2$, respectively, indicating a higher permeability to Li^+ over other cations (Figure 3A). In contrast, COF-OHep-PAN exhibited an ion transport selectivity trend of $K^+ > Na^+ > Li^+ > Mg^{2+} > Ca^{2+}$, in agreement with their intrinsic ion transmission efficiency (Figure 3B).[10] These results verified the high activity of the oligoether-mediated transport of Li ions.[22–27]

To investigate the separation of lithium and magnesium, ion transport kinetics measurements were conducted to further demonstrate the ability of COF-4EO-PAN to selectively transport Li^+ over Mg^{2+} across the membrane. The experiments were

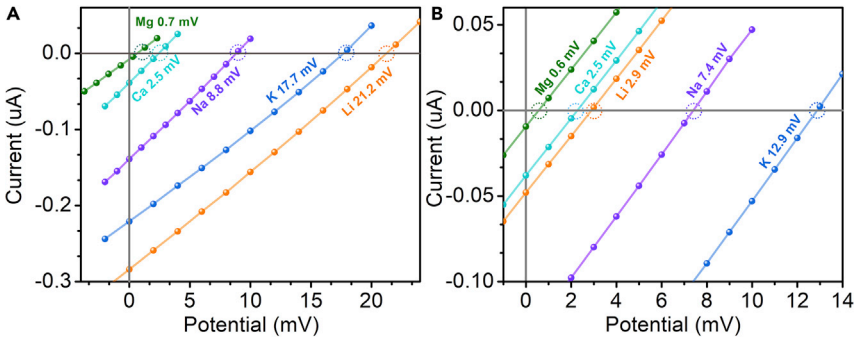

Figure 3. Relative ion permeability investigation

Current-voltage plots for (A) COF-4EO-PAN and (B) COF-OHep-PAN under asymmetrical salt solutions, with the *cis* side being filled with $MgCl_2$ aqueous solution and the *trans* side being filled with KCl, NaCl, LiCl, $MgCl_2$, or $CaCl_2$. The concentration of Cl ions was maintained at 1 mM.

conducted at room temperature using a homemade diffusion cell, wherein the feed and permeate chambers were filled with an aqueous salt solution and deionized water, respectively. The ion concentration in the permeate chamber was analyzed at different time intervals by ion chromatography (Figure S14), with each point measured three times in parallel. As shown in Figure 4, the concentrations of both Li^+ and Mg^{2+} ions increased linearly over time, and the slope for Li^+ was much steeper than that of Mg^{2+}, indicative of the higher permeability to Li^+ over Mg^{2+} across the membrane. A Li^+/Mg^{2+} separation factor of 12 was obtained by dividing the slopes. In contrast, COF-OHep-PAN afforded a Li^+/Mg^{2+} separation factor of only 3 under otherwise identical conditions (Figures S15 and S16).

To understand the chemical basis of the binding selectivity of COF-4EO-PAN toward Li^+ over Mg^{2+}, quantum density functional theory computations were performed. Calculations of the truncated fragments shown in Figure S17 were performed using M062X exchange and correlation functions, and a 6-311G* basis was used for all atoms. The binding free energies for Li^+ and Mg^{2+} to the oligoether were computed using the quasi-chemical method and showed that the oligoether moiety exhibits a higher binding affinity toward Li^+ over Mg^{2+} by 55.5 kJ mol^{-1} in aqueous solution (Table S5). We performed X-ray photoelectron spectroscopy (XPS) to analyze the interaction between Li^+ and the oligoethers. The binding energy of lithium species in Li^+@COF-4EO (55.9 eV) is lower than that in LiCl (56.6 eV), reflecting the electron transfer from the ethylene oxide moiety to the Li ions (Figure S18). To further understand the Li^+ transport processes in COF-4EO-PAN, the dynamic behavior of Li ions in the COF channels was studied by static solid-state ^{7}Li NMR spectroscopy. We collected the spectra of LiCl and Li@COF-OHep (COF-OHep is the corresponding powder form of COF-OHep-PAN) as references to show the spectroscopic behavior of Li species in a solid matrix with minimal mobility and in a porous material with no lithium binding sites, which gave rise to very broad peaks centered at −1.53 ppm. In contrast, a narrower ^{7}Li NMR signal was detected for COF-4EO, suggestive of the weakened solid-state couplings and hence the higher mobility (Figure S19).[24]

From the characterization results, we concluded that the oxygen atoms in the oligoether moieties replace the oxygen atoms in water and coordinate with the Li ion. The oligoether moieties thus act like surrogate water, with the energetic costs of dehydration balanced by the energy gains from coordination with oxygen atoms (in bulk aqueous solution there are four and six water molecules coordinated with each Li or Mg ion, respectively, in the first hydration shell).[56] This process may be

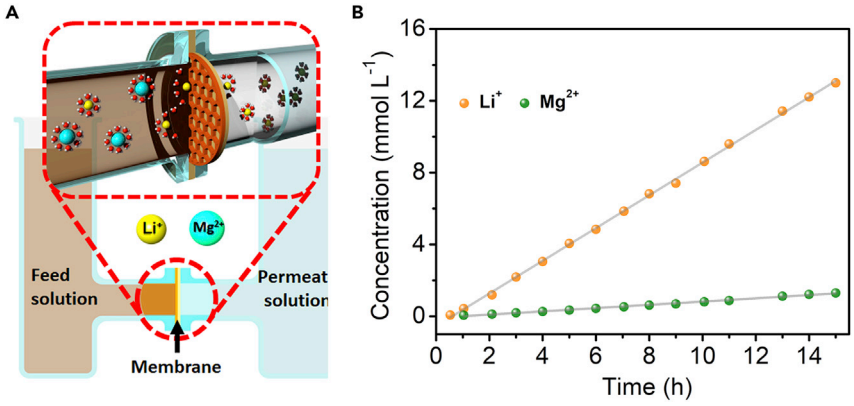

Figure 4. Li^+/Mg^{2+} separation performance evaluation

(A) Schematic diagram of ion permeation through COF-4EO-PAN in a homemade diffusion cell, with a binary salt solution containing LiCl and $MgCl_2$ as the feed solution and H_2O as the permeate solution.

(B) The concentration change of a single salt (0.1 M LiCl or 0.1 M $MgCl_2$) through the membrane to the opposite side as a function of time for COF-4EO-PAN. The ion concentrations were determined by ion chromatography.

further facilitated by the hydrophobic COF active layer, as revealed by the contact-angle measurements (Figure S20). The alkyl chain exhibited no specific affinity for Li ions, thus giving rise to an inferior selective permeation. However, the mechanism of the conduction of Li ions through the COF channels was still unclear, as the characterization results implied that a single Li ion would be held very tightly within the membrane. To understand this, we evaluated the Li^+ concentration in COF-4EO-PAN by measuring the transmembrane ionic conductance. The membrane was squeezed between two reservoirs containing symmetric salt solutions of various concentrations. The measured ionic conductance deviated from the bulk values, suggesting that the Li ions are enriched in the pore channels (Figure 5A).[11] The high concentration of the densely coordinated Li ions in the pore channel results in mutual repulsion, which overcomes the otherwise strong interaction between the oligoether and the Li ion, thereby promoting the transport of Li^+ along the direction of the concentration gradient. The transmembrane ionic conductance of Mg^{2+} was close to that of the bulk electrolyte solution, confirming the ability of COF-4EO-PAN to facilitate the transport of Li ions (Figure 5B). Therefore, we could confirm strong interactions between Li ions and the lithiophilic oligoether arms, as well as a high throughput mediated by concentration gradient-driven transport. A tentative transport mechanism was proposed: the rapid and reversible complexation between the oligoether moiety and the Li^+ together with the dynamic environment created by the aligned oligoether chains, which allows the ions to move from one binding site to the next, selectively augments the transport of Li ions through the membrane.

After confirming the role of the aligned oligoethers on conferring ion selectivity, we further investigated their impact on the ion transport activity. Interestingly, even with COF-4EO-PAN having much more crowded pore channels than COF-2,5-dimethoxyterephthalaldehyde (OMe)-PAN (there is only one methoxyl group branching off the phenyl ring, Figures 2D and S21–S25), both afforded comparable Li ion transport rates, which were much faster than that of COF-OHep-PAN. In contrast to the Li ions, the permeation of Mg ions is in good accordance with the free space of the pore channels, decreasing in the order COF-OMe-PAN > COF-OHep-PAN > COF-4EO-PAN, with more extended substitution groups giving a lower flux. These results

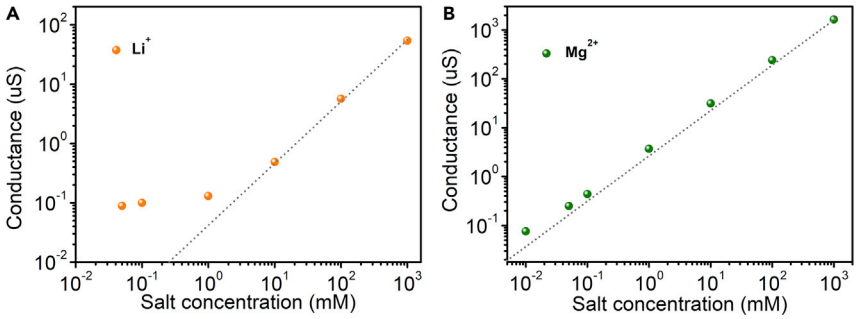

Figure 5. Ion transmembrane conductance investigation

(A) The transmembrane Li conductance apparently deviates from the bulk value (dashed line) from below ~1 mM, whereas (B) the transmembrane Mg conductance is close to that of the bulk solution for COF-4EO-PAN.

confirm that lithiophilic oligoethers facilitate the transport of Li ions, but obstruct the Mg ions from moving through the membrane channels. Given their comparable thickness and pore structure, we concluded that the significant disparity in Li^+/Mg^{2+} selectivity between COF-4EO-PAN and COF-OHep-PAN originates from the densely populated lithiophilic arms in COF-4EO-PAN, which could arrange into a transport pathway, allowing the diffusion of Li ions, reminiscent of that seen in cellular membranes (Figures S15 and S16).

We further tested the lithium extraction efficiency of COF-4EO-PAN using a mixture of LiCl (0.1 M) and $MgCl_2$ (0.1 M) aqueous solutions. Figure 6A shows the selectivity profile and the concentrations of Li and Mg ions in the permeate solution as a function of time. The Li^+ and Mg^{2+} concentrations increased with time. The Li^+/Mg^{2+} ratio over COF-4EO-PAN increased during the initial 2 h, reaching its maximum value of 64, and then slightly decreased. The higher binary Li^+/Mg^{2+} selectivity compared with the ideal selectivity can be ascribed to the competitive coordination between the oligoether moiety and the Li and Mg ions. To better understand this process, the real-time fluxes of Li and Mg ions were calculated. It was observed that the flux of Li ions was always much greater than that of Mg ions, validating the higher affinity of COF-4EO-PAN toward Li species (Figure S26). The increased flux of Mg^{2+} after 2 h could be attributed to the tendency of permeation to reach equilibrium and concentration-dependent competing interactions with binding sites, thus resulting in decreased selectivity. The observed relatively lengthy induction period (2 h) may be a disadvantage during actual application, but offers the opportunity to manipulate performance combinations to match process scale requirements.

Given that the concentration gradient is the driving force of dialysis, an increase in feed concentration is expected to enhance permeability and, consequently, the efficiency. With the rise in the concentration of feed solution from 0.01 to 1.0 M, the flux of Li^+ through COF-4EO-PAN increased from 6.8 to 230 mmol m^{-2} h^{-1}, while the selectivity was retained (Figures S27 and S28). This offers an advantage over the state-of-the-art charge-modified membranes, where increasing the salinity usually results in partial or complete loss in selectivity. To further test the applicability of COF-4EO-PAN for lithium mining from various systems, the impact of solution pH on the Li^+/Mg^{2+} separation performance was investigated. Considering that Li and Mg species are inclined to precipitate out in the form of hydroxide, the lithium extraction performance under pH values ranging from 2.5 to 6.1 was evaluated, which revealed that the separation factor increases along with the increase in solution pH (Figure S29). This is because the ether oxygen species may be protonated under low

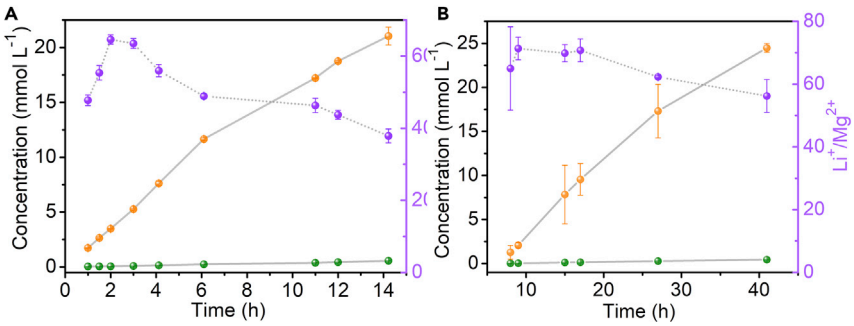

Figure 6. Binary salt separation performance test

Lithium and magnesium separation performance tests for COF-4EO-PAN in a closed system and a cycling system. The concentration change of binary salt (0.1 M LiCl and 0.1 M $MgCl_2$) through COF-4EO-PAN to the permeate chamber and the corresponding separation factor as a function of time in (A) a closed system and (B) a cycling system is shown (orange, Li^+; olive, Mg^{2+}; violet, Li^+/Mg^{2+}). The error bars are obtained from the average of three different batches.

pH conditions, thereby reducing the coordination ability of the oligoether moieties toward Li^+.

We further assessed the stability of COF-4EO-PAN by evaluating its performance over multiple cycles, which is an essential feature of any system considered for use in industrial applications. A new feed solution and deionized water were used. A negligible decrease in selectivity and flux was observed after five cycles, providing evidence of the robustness of the membrane. Another major concern is that in low-grade salt lakes, the Mg^{2+}/Li^+ ratio is up to 30. As we demonstrated, this could be addressed by connecting a number of permeate chambers in series. For example, with a feed solution having a Mg^{2+}/Li^+ ratio of 30, the ratio reached approximately 0.5 in the second permeate chamber. For practical applications, continuous dialysis is preferred over batch dialysis. To demonstrate the applicability of COF-4EO-PAN in continuous dialysis, the ratio of Li^+/Mg^{2+} was tested cyclically. After testing for at least 40 h, only a slight decrease in selectivity was observed (Figure 6B).

DISCUSSION

In summary, we have described the fabrication of lithium ion nanochannels in COF membranes, exhibiting remarkably high selectivity for Li ions. The unique channel system features the following: (1) densely aligned lithiophilic oligoether moieties enrich Li ions in the pore channel; (2) the flexibility of oligoethers facilitates their coordination with Li ions and lowers the energy barrier of ion transport across the membrane; and (3) increased channel congestion resulting from the introduced oligoethers has little effect on the Li^+ transport activity but obstructs the other ions from entering the channel, resulting in high selectivity. We believe that the versatility of the pore environment paired with the pore-structure engineering of COF materials provides a new avenue to achieve a better understanding of ion transport processes and, thereby, will lead to rational design principles to address the bottlenecks in the further development of membrane technology for separation.

EXPERIMENTAL PROCEDURES

Resource availability

Lead contact

Further information and requests for resources and materials should be directed to and will be fulfilled by the lead contact, Qi Sun (sunqichs@zju.edu.cn).

Materials availability

This study did not generate new unique reagents. Chemicals used for synthesis of monomers were purchased from Aladdin and used directly without any purification unless mentioned. The purity of the monomers used for COF synthesis was determined by NMR analyses (Figure S30). The asymmetric PAN ultrafiltration membrane with a molecular weight cutoff of 40,000 Da was obtained from Sepro Membranes (Carlsbad, CA, USA).

Date and code availability

All data needed to evaluate the conclusions in the paper are present in the paper and/or the supplemental information. Additional data related to this study are available from the corresponding authors upon reasonable request.

Fabrication of membranes

COF-4EO-PAN

The COF-4EO active layer was formed via interface polymerization on the surface of a PAN ultrafiltration membrane. The PAN support was vertically placed in the middle of a homemade diffusion cell, resulting in a volume of 17 cm^3 each (see Figure S1). An aqueous solution of TAB (15.9 mg, 0.045 mmol) dissolved in 3 M acetic acid (17 mL) and an organic phase with 4EO (31.2 mg, 0.068 mmol) dissolved in a mixture of ethyl acetate and mesitylene (vol/vol = 3/1, 17 mL) were separately introduced into the two sides of the diffusion cell. The reaction mixture was kept at 30°C for 4 days. The resulting membrane was rinsed with the mixture of ethyl acetate and mesitylene, and methanol, in sequence, to remove any residual monomers, catalyst, and organic solvents. Finally, each membrane was rinsed with water for 24 h and then used for permeation tests or air-dried for physicochemical characterization. Atomistic coordinates for the AA-stacking mode of COF-OMe optimized using the Forcite method are listed in Table S2.

COF-OHep-PAN

The COF-OHep active layer was formed via interface polymerization on the surface of an asymmetric PAN. The PAN support was vertically placed in the middle of a homemade diffusion cell, resulting in a volume of 17 cm^3 each. An aqueous solution of TAB (15.9 mg, 0.045 mmol) dissolved in 3 M acetic acid (17 mL) and an organic phase with OHep (12.3 mg, 0.034 mmol) dissolved in a mixture of *n*-BuOH and *o*-dichlorobenzene (vol/vol = 3/1, 17 mL) were separately introduced into the two sides of the diffusion cell. The reaction mixture was kept at 30°C for 4 days. The resulting membrane was rinsed with the mixture of ethyl acetate and mesitylene, and methanol, in sequence, to remove any residual monomers, catalyst, and organic solvents. Finally, each membrane was rinsed with water for 24 h and then used for permeation tests or air-dried for physicochemical characterization. Atomistic coordinates for the AA-stacking mode of COF-OMe optimized using the Forcite method are listed in Table S3.

COF-OMe-PAN

The COF-OMe active layer was formed via interface polymerization on the surface of an asymmetric PAN. The PAN support was vertically placed in the middle of a homemade diffusion cell, resulting in a volume of 17 cm^3 each. An aqueous solution of TAB (15.9 mg, 0.045 mmol) dissolved in 3 M acetic acid (17 mL) and an organic phase with OMe (13.2 mg, 0.068 mmol) dissolved in a mixture of ethyl acetate and mesitylene (vol/vol = 3/1, 17 mL) were separately introduced into the two sides of the diffusion cell. The reaction mixture was kept at 30°C for 4 days. The resulting membrane was rinsed with the mixture of ethyl acetate and mesitylene, and methanol, in

sequence, to remove any residual monomers, catalyst, and organic solvents. Finally, each membrane was rinsed with water for 24 h and then used for permeation tests or air-dried for physicochemical characterization. Atomistic coordinates for the AA-stacking mode of COF-OMe optimized using Forcite method are listed in Table S4.

Characterization

The N_2 sorption isotherms were measured at 77 K using a liquid N_2 bath. PXRD data were collected on a Bruker AXS D8 Advance A25 powder X-ray diffractometer (40 kV, 40 mA) using Cu Kα (λ = 1.5406 Å) radiation. SEM images were collected using a Hitachi SU 8010. FTIR spectra were recorded on a Nicolet Impact 410 FTIR spectrometer. Inductively coupled plasma optical emission spectroscopy was performed on a PerkinElmer Elan DRC II quadrupole. XPS spectra were performed on a Thermo ESCALAB 250 with Al Kα irradiation at θ = 90° for X-ray sources, and the binding energies were calibrated using the C1s peak at 284.9 eV. ^{1}H NMR spectra were recorded on a Bruker Avance-400 (400 MHz) spectrometer. Chemical shifts are expressed in parts per million downfield from TMS at δ = 0 ppm, and *J* values are given in Hz. Static solid-state ^{7}Li NMR experiments were recorded on a Bruker Avance 500 spectrometer equipped with a magic-angle spin probe in a 4-mm ZrO_2 rotor. GIWAXS measurements were conducted on a MicroMax-007HF with a high-intensity microfocus rotating anode X-ray generator at an incident angle of 0.2°. The samples were recorded in the 2θ range of 2°–40° and the data were collected with Win software. Two-dimensional GIWAXS was conducted to analyze the orientation of the COF layer by using a XEUSS SAXS/WAXS system at an incident angle of 0.2°. The membrane samples were cut into small pieces (1 × 1 cm) and then attached to a silicon wafer. The 2D GIWAXS data of membranes were evaluated using a MarCDD X-ray detector.

SUPPLEMENTAL INFORMATION

Supplemental information can be found online at https://doi.org/10.1016/j.matt.2021.03.017.

ACKNOWLEDGMENTS

The authors acknowledge the National Science Foundation of China (21776241, 2196116074, 222071132) and the Fundamental Research Funds for the Central Universities (17221012001). Partial support from the Robert A. Welch Foundation (B-0027) is also acknowledged (S.M.).

AUTHOR CONTRIBUTIONS

Q.S., S.M., and L.Z. conceived and designed the research. S.B., W.X., S.C., and L.H. performed the synthesis and carried out the separation tests. Y.S. contributed to the XRD test. X.L. performed and analyzed the solid-state ^{7}Li NMR. All authors participated in drafting the paper and gave approval to the final version of the manuscript.

DECLARATION OF INTERESTS

The authors declare no competing interests.

Received: December 17, 2020
Revised: February 22, 2021
Accepted: March 17, 2021
Published: April 7, 2021

REFERENCES

1. Tu, Y.-M., Song, W., Ren, T., Shen, Y.-X., Chowdhury, R., Rajapaksha, P., Culp, T.E., Samineni, L., Lang, C., Thokkadam, A., et al. (2020). Rapid fabrication of precise high-throughput filters from membrane protein nanosheets. Nat. Mater. *19*, 347–354.
2. Gouaux, E., and MacKinnon, R. (2005). Principles of selective ion transport in channels and pumps. Science *310*, 1461–1465.
3. Doyle, D.A., Cabral, J.M., Pfuetzner, R.A., Kuo, A., Gulbis, J.M., Cohen, S.L., Chait, B.T., and MacKinnon, R. (1998). The structure of the potassium channel: molecular basis of K^+ conduction and selectivity. Science *280*, 69–77.
4. He, X., Yang, Y., Wu, H., He, G., Xu, Z., Kong, Y., Cao, L., Shi, B., Zhang, Z., Tongsh, C., et al. (2020). De novo design of covalent organic framework membranes toward ultrafast Anion transport. Adv. Mater. *32*, 2001284.
5. Guo, Y., Ying, Y., Mao, Y., Peng, X., and Chen, B. (2016). Polystyrene sulfonate threaded through a metal-organic framework membrane for fast and selective lithium-ion separation. Angew. Chem. Int. Ed. *55*, 15120–15124.
6. Tan, R., Wang, A., Malpass-Evans, R., Williams, R., Zhao, E.W., Liu, T., Ye, C., Zhou, X., Darwich, B.P., Fan, Z., et al. (2020). Hydrophilic microporous membranes for selective ion separation and flow-battery energy storage. Nat. Mater. *19*, 195–202.
7. Shehzad, M.A., Wang, Y., Yasmin, A., Ge, X., He, Y., Liang, X., Zhu, Y., Hu, M., Xiao, X., Ge, L., et al. (2019). Biomimetic nanocones that enable high ion permselectivity. Angew. Chem. Int. Ed. *58*, 12646–12654.
8. Zhang, M., Guan, K., Ji, Y., Liu, G., Jin, W., and Xu, N. (2019). Controllable ion transport by surface-charged graphene oxide membrane. Nat. Commun. *10*, 1253.
9. Li, X., Zhang, H., Yu, H., Xia, J., Zhu, Y.-B., Wu, H.-A., Hou, J., Lu, J., Ou, R., Easton, C.D., et al. (2020). Unidirectional and selective proton transport in artificial heterostructured nanochannels with nano-to-subnano confined water clusters. Adv. Mater. *32*, 2001777.
10. Lu, J., Zhang, H., Hou, J., Li, X., Hu, X., Hu, Y., Easton, C.D., Li, Q., Sun, C., Thornton, A.W., et al. (2020). Efficient metal ion sieving in rectifying subnanochannels enabled by metal-organic frameworks. Nat. Mater. *19*, 767–774.
11. Ding, L., Xiao, D., Lu, Z., Deng, J., Wei, Y., Caro, J., and Wang, H. (2020). Oppositely charged $Ti_3C_2T_x$ MXene membranes with 2D nanofluidic channels for osmotic energy harvesting. Angew. Chem. Int. Ed. *59*, 8720–8726.
12. Tagliazucchi, M., Peleg, O., Kroger, M., Rabin, Y., and Szleifer, I. (2013). Effect of charge, hydrophobicity, and sequence of nucleoporins on the translocation of model particles through the nuclear pore complex. Proc. Nat. Acad. Sci. U S A. *110*, 3363–3368.
13. Nishizawa, M., Menon, V.P., and Martin, C.R. (1995). Metal nanotubule membranes with electrochemically switchable ion-transport selectivity. Science *268*, 700–702.
14. Razmjou, A., Asadnia, M., Hosseini, E., Korayem, A.H., and Chen, V. (2019). Design principles of ion selective nanostructured membranes for the extraction of lithium ions. Nat. Commun. *10*, 5793.
15. Yang, S., Zhang, F., Ding, H., He, P., and Zhou, H. (2018). Lithium metal extraction from seawater. Joule *2*, 1648–1651.
16. Choubey, P.K., Kim, M.-s., Srivastava, R.R., Lee, J.-c., and Lee, J.-Y. (2016). Advance review on the exploitation of the prominent energy-storage element: lithium. Part I: from mineral and brine resources. Miner. Eng. *89*, 119–137.
17. Vikström, H., Davidsson, S., and HööK, M. (2013). Lithium availability and future production outlooks. Appl. Energ. *110*, 252–266.
18. Li, X., Zhang, C., Zhang, S., Li, J., He, B., and Cui, Z. (2015). Preparation and characterization of positively charged polyamide composite nanofiltration hollow fiber membrane for lithium and magnesium separation. Desalination *369*, 26–36.
19. Childress, A.E., and Elimelech, M. (2000). Relating nanofiltration membrane performance to membrane charge (electrokinetic) characteristics. Environ. Sci. Technol. *34*, 3710–3716.
20. Somrani, A., Hamzaoui, A.H., and Pontie, M. (2013). Study on lithium separation from salt lake brines by nanofiltration (NF) and low pressure reverse osmosis (LPRO). Desalination *317*, 184–192.
21. Ge, L., Wu, B., Li, Q., Wang, Y., Yu, D., Wu, L., Pan, J., Miao, J., and Xu, T. (2016). Electrodialysis with nanofiltration membrane (EDNF) for high-efficiency cations fractionation. J. Membr. Sci. *498*, 192–200.
22. Gadjourova, Z., Andreev, Y.G., Tunstall, D.P., and Bruce, P.G. (2001). Ionic conductivity in crystalline polymer electrolytes. Nature *412*, 520–523.
23. Webb, M.A., Jung, Y., Pesko, D.M., Savoie, B.M., Yamamoto, U., Coates, G.W., Balsara, N.P., Wang, Z.-G., and Miller, T.F., III (2015). Systematic computational and experimental investigation of lithium-ion transport mechanisms in polyester-based polymer electrolytes. ACS Cent. Sci. *1*, 198–205.
24. Zhang, G., Hong, Y.-l., Nishiyama, Y., Bai, S., Kitagawa, S., and Horike, S. (2019). Accumulation of glassy poly(ethylene oxide) anchored in a covalent organic framework as a solid-state Li^+ electrolyte. J. Am. Chem. Soc. *141*, 1227–1234.
25. Guo, Z., Zhang, Y., Yu, D., Li, J., Li, S., Shao, P., Feng, X., and Wang, B. (2019). Fast ion transport pathway provided by polyethylene glycol confined in covalent organic frameworks. J. Am. Chem. Soc. *141*, 1923–1927.
26. Xie, Z., Wang, B., Yang, Z., Yang, X., Yu, X., Xing, G., Zhang, Y., and Chen, L. (2019). Stable 2D heteroporous covalent organic frameworks for efficient ionic conduction. Angew. Chem. Int. Ed. *58*, 15742–15746.
27. Xu, Q., Tao, S., Jiang, Q., and Jiang, D. (2018). Ion conduction in polyelectrolyte covalent organic frameworks. J. Am. Chem. Soc. *140*, 7429–7432.
28. Song, Y., Sun, Q., Aguila, B., and Ma, S. (2019). Opportunities of covalent organic frameworks for advanced applications. Adv. Sci. *6*, 1801410.
29. Geng, K., He, T., Liu, R., Dalapati, S., Tan, K., Li, Z., Tao, S., Gong, Y., Jiang, Q., and Jiang, D. (2020). Covalent organic frameworks: design, synthesis, and functions. Chem. Rev. *120*, 8814–8933.
30. Guan, X., Chen, F., Fang, Q., and Qiu, S. (2020). Design and applications of three dimensional covalent organic frameworks. Chem. Soc. Rev. *49*, 1357–1384.
31. Wang, Z., Zhang, S., Chen, Y., Zhang, Z., and Ma, S. (2020). Covalent organic frameworks for separation applications. Chem. Soc. Rev. *49*, 708–735.
32. Kandambeth, S., Dey, K., and Banerjee, R. (2019). Covalent organic frameworks: chemistry beyond the structure. J. Am. Chem. Soc. *141*, 1807–1822.
33. Lohse, M.S., and Bein, T. (2018). Covalent organic frameworks: structures, synthesis, and applications. Adv. Funct. Mater. *28*, 1705553.
34. Jin, Y., Hu, Y., and Zhang, W. (2017). Tessellated multiparous two-dimensional covalent organic frameworks. Nat. Rev. Chem. *1*, 0056.
35. Guan, X., Li, H., Ma, Y., Xue, M., Fang, Q., Yan, Y., Valtchev, V., and Qiu, S. (2019). Chemically stable polyarylether-based covalent organic frameworks. Nat. Chem. *11*, 587–594.
36. Sasmal, H.S., Halder, A., Kunjattu H, S., Dey, K., Nadol, A., Ajithkumar, T.G., Bedadur, P.R., and Banerjee, R. (2019). Covalent self-assembly in two dimensions: connecting covalent organic framework nanospheres into crystalline and porous thin films. J. Am. Chem. Soc. *141*, 20371–20379.
37. Yuan, C., Wu, X., Gao, R., Han, X., Liu, Y., Long, Y., and Cui, Y. (2019). Nanochannels of covalent organic frameworks for chiral selective transmembrane transport of amino acids. J. Am. Chem. Soc. *141*, 20187–20197.
38. Hao, Q., Li, Z.-J., Lu, C., Sun, B., Zhong, Y.-W., Wan, L.-J., and Wang, D. (2019). Oriented two-dimensional covalent organic framework films for near-infrared electrochromic application. J. Am. Chem. Soc. *141*, 19831–19838.
39. Yang, H., Yang, L., Wang, H., Xu, Z., Zhao, Y., Luo, Y., Nasir, N., Song, Y., Wu, H., Pan, F., and Jiang, Z. (2019). Covalent organic framework membranes through a mixed-dimensional assembly for molecular separations. Nat. Commun. *10*, 2101.
40. Wang, R., Shi, X., Xiao, A., Zhou, W., and Wang, Y. (2018). Interfacial polymerization of covalent organic frameworks (COFs) on polymeric substrates for molecular separations. J. Membr. Sci. *566*, 197–204.
41. Shinde, D.B., Sheng, G., Li, X., Ostwal, M., Emwas, A.-H., Huang, K.-W., and Lai, Z. (2018). Crystalline 2D covalent organic framework membranes for high-flux organic solvent

nanofiltration. J. Am. Chem. Soc. *140*, 14342–14349.

42. Ratsch, M., Ye, C., Yang, Y., Zhang, A., Evans, A., and Borjesson, K. (2020). All-carbon-linked continuous three-dimensional porous aromatic framework films with nanometer-precise controllable thickness. J. Am. Chem. Soc. *142*, 6548–6553.

43. Kuehl, V.A., Yin, J., Duong, P.H.H., Mastorovich, B., Newell, B., Li-Oakey, K.D., Parkinson, B.A., and Hoberg, J.O. (2018). A highly ordered nanoporous, two-dimensional covalent organic framework with modifiable pores, and its application in water purification and ion sieving. J. Am. Chem. Soc. *140*, 18200–18207.

44. Fan, H., Mundstock, A., Feldhoff, A., Knebel, A., Gu, J., Meng, H., and Caro, J. (2018). Covalent organic framework-covalent organic framework bilayer membranes for highly selective gas separation. J. Am. Chem. Soc. *140*, 10094–10098.

45. Li, Y., Guo, X., Li, X., Zhang, M., Jia, Z., Deng, Y., Tian, Y., Li, S., and Ma, L. (2020). Redox-active two-dimensional covalent organic frameworks (COFs) for selective reductive separation of valence-variable, redox-sensitive and long-lived radionuclides. Angew. Chem. Int. Ed. *59*, 4168–4175.

46. Ying, Y., Tong, M., Ning, S., Ravi, S.K., Peh, S.B., Tan, S.C., Pennycook, S.J., and Zhao, D. (2020). Ultrathin two-dimensional membranes assembled by ionic covalent organic nanosheets with reduced apertures for gas separation. J. Am. Chem. Soc. *142*, 4472–4480.

47. Li, X., Cai, S., Sun, B., Yang, C., Zhang, J., and Liu, Y. (2020). Chemically robust covalent organic frameworks: progress and perspective. Mater *3*, 1507–1540.

48. Hou, L., Xian, W., Bing, S., Song, Y., Sun, Q., Zhang, L., and Ma, S. (2021). Understanding the ion transport behavior across nanofluidic membranes in response to the charge variations. Adv. Funct. Mater. 2009970, https://doi.org/10.1002/adfm.202009970.

49. Xu, H., Gao, J., and Jiang, D. (2015). Stable, crystalline, porous, covalent organic frameworks as a platform for chiral organocatalysts. Nat. Chem. *7*, 905–912.

50. Sun, Q., Tang, Y., Aguila, B., Wang, S., Xiao, F.-S., Thallapally, P.K., Al-Enizi, A.M., Nafady, A., and Ma, S. (2019). Reaction environment modification in covalent organic frameworks for catalytic performance enhancement. Angew. Chem. Int. Ed. *58*, 8670–8675.

51. Ratner, M.A., and Shriver, D.F. (1988). Ion transport in solvent-free polymer. Chem. Rev. *88*, 109–124.

52. Dong, R., Zhang, T., and Feng, X. (2018). Interface-assisted synthesis of 2D materials: trend and challenges. Chem. Rev. *118*, 6189–6235.

53. Sun, Q., Aguila, B., Lan, P.C., and Ma, S. (2019). Tuning pore heterogeneity in covalent organic frameworks for enhanced enzyme accessibility and resistance against denaturants. Adv. Mater. *31*, 1900008.

54. Colson, J.W., Woll, A.R., Mukherjee, A., Levendorf, M.P., Spitler, E.L., Shields, V.B., Spencer, M.G., Park, J., and Dichtel, W.R. (2011). Oriented 2D covalent organic framework thin films on single-layer graphene. Science *332*, 228–231.

55. Sparreboom, W., van den Berg, A., and Eijkel, J.C.T. (2009). Principles and applications of nanofluidic transport. Nat. Nanotechnol. *4*, 713–720.

56. Marcus, Y. (2009). Effect of ions on the structure of water: structure making and breaking. Chem. Rev. *109*, 1346–1370.